Kuiper belts around nearby stars

A&A 518, A40 (2010)
DOI: 10.1051/0004-6361/201014444

Astronomy & Astrophysics

Kuiper belts around nearby stars⋆

R. Nilsson[1], R. Liseau[2], A. Brandeker[1], G. Olofsson[1], G. L. Pilbratt[3], C. Risacher[4], J. Rodmann[5], J.-C. Augereau[6], P. Bergman[2], C. Eiroa[7], M. Fridlund[3], P. Thébault[8,1], and G. J. White[9,10]

[1] Department of Astronomy, Stockholm University, AlbaNova University Center, Roslagstullsbacken 21, 106 91 Stockholm, Sweden
e-mail: [ricky;alexis;olofsson]@astro.su.se
[2] Onsala Space Observatory, Chalmers University of Technology, SE-439 92 Onsala, Sweden
e-mail: [rene.liseau;per.bergman]@chalmers.se
[3] ESA Astrophysics Missions Division, ESTEC, PO Box 299, 2200 AG Noordwijk, The Netherlands
e-mail: malcolm.fridlund@esa.int; gpilbratt@rssd.esa.int
[4] SRON, Postbus 800, 9700 AV Groningen, The Netherlands
e-mail: crisache@sron.nl
[5] ESA/ESTEC Space Environment and Effects Section, PO Box 299, 2200 AG Noordwijk, The Netherlands
e-mail: jens.rodmann@esa.int
[6] Université Joseph Fourier/CNRS, Laboratoire d'Astrophysique de Grenoble, UMR 5571, Grenoble, France
e-mail: augereau@obs.ujf-grenoble.fr
[7] Dpto. Física Teórica, Facultad de Ciencias, Universidad Autónoma de Madrid, 28049 Madrid, Spain
e-mail: carlos.eiroa@uam.es
[8] Observatoire de Paris, Section de Meudon, 92195 Meudon Principal Cedex, France
e-mail: philippe.thebault@obspm.fr
[9] Department of Physics and Astronomy, Open University, Walton Hall, Milton Keynes MK7 6AA, UK
e-mail: g.j.white@open.ac.uk
[10] Science and Technology Facilities Council, Rutherford Appleton Laboratory, Chilton, Didcot OX11 0QX, UK

Received 17 March 2010 / Accepted 18 May 2010

ABSTRACT

Context. The existence of dusty debris disks around a large fraction of solar type main-sequence stars, inferred from excess far-IR and submillimetre emission compared to that expected from stellar photospheres, suggests that leftover planetesimal belts analogous to the asteroid- and comet reservoirs of the solar system are common.
Aims. Sensitive submillimetre observations are essential to detect and characterise cold extended dust originating from collisions of small bodies in disks, belts, or rings at Kuiper-belt distances (30–50 AU or beyond). Measurements of the flux densities at these wavelengths will extend existing IR photometry and permit more detailed modelling of the Rayleigh-Jeans tail of the disks spectral energy distribution (SED), effectively constraining dust properties and disk extensions. By observing stars spanning from a few up to several hundred Myr, the evolution of debris disks during crucial phases of planet formation can be studied.
Methods. We observed 22 exo-Kuiper-belt candidates at 870 μm, as part of a large programme with the LABOCA bolometer at the APEX telescope. Dust masses (or upper limits) were calculated from integrated 870 μm fluxes, and fits to the SED of detected sources revealed the fractional dust luminosities $f_{\rm dust}$, dust temperatures $T_{\rm dust}$, and power-law exponents β of the opacity law.
Results. A total of 10 detections with at least 3σ significance were made, out of which five (HD 95086, HD 131835, HD 161868, HD 170773, and HD 207129) have previously never been detected at submillimetre wavelengths. Three additional sources are marginally detected with >2.5σ significance. The best-fit β parameters all lie between 0.1 and 0.8, in agreement with previous results indicating the presence of significantly larger grains than those in the ISM. From our relatively small sample we estimate $f_{\rm dust} \propto t^{-\alpha}$, with $\alpha \sim 0.8-2.0$, and identify an evolution of the characteristic radial dust distance $R_{\rm dust}$ that is consistent with the $t^{1/3}$ increase predicted from models of self-stirred collisions in debris disks.

Key words. circumstellar matter – planetary systems – planets and satellites: formation – Kuiper belt: general – submillimeter: planetary systems

1. Introduction

The existence of warm dust around solar type main-sequence stars is implied from infrared (IR) excess emission (above the stellar photospheric contribution) discovered by the *Infrared Astronomical Satellite* (IRAS, e.g. Aumann et al. 1984; Neugebauer et al. 1984), and studied by the *Infrared Space Observatory* (ISO, e.g. Kessler et al. 1996), and *Spitzer* (e.g. Werner et al. 2004). Since such dust has a limited lifetime, its existence suggests there are larger asteroidal and/or cometary bodies that continuously replenish the dusty debris disk through collisions. Excess emission at wavelengths of 25 μm and shorter comes predominantly from hot dust (>300 K), located within 1–5 AU of the star (similar to the asteroidal belt in our solar system), while an excess at 25–100 μm probes cooler dust (~100–300 K) located at 5–10 AU. However, to detect cold and

⋆ Based on observations with APEX, Llano Chajnantor, Chile (OSO programme 081.F-9330(A)).

very extended dust, originating in Kuiper-belt analogues (of the order of 100 AU from the star), observations at submillimetre (submm) wavelengths are needed. Although very few older stars show evidence of hot dust, likely due to clearing by planets (e.g. Beichman et al. 2006b; Meyer et al. 2008), cool debris disks appear more common and many should be detectable at submm wavelengths based on extrapolation from observed far-IR fluxes.

The potential correlation of cold dust and planetesimal belts with the formation of exoplanets in these systems is another incentive for broader submm surveys of nearby solar-type main-sequence stars. Beichman et al. (2006a) and Bryden et al. (2006) reported *Spitzer* MIPS observations of a large sample of nearby F, G, and K main-sequence stars, and detected an overall excess of 70 μm emission towards 13% of the stars. A larger sample of solar-type stars, spanning ages between 3 Myr and 3 Gyr, studied in the *Spitzer* Legacy programme Formation and Evolution of Planetary Systems (FEPS), showed a total 70 μm excess rate of 7% with high (50 times the photosphere) fractional excesses at ages between 30 and 200 Myr, and significantly lower fractional excess for older stars (Carpenter et al. 2009; Hillenbrand et al. 2008). There was no clear trend for the temporal evolution of 70 μm excess in FEPS, however Su et al. (2006) estimate a decay time of ~400 Myr for A type stars. At submm and mm wavelengths 3% of the FEPS stars show evidence of continuum emission, with a suggested decrease in dust masses and/or changes in the grain properties for stellar ages of 10−30 Myr (Carpenter et al. 2005).

An additional advantage in making observations in the submm region is that measured integrated fluxes are directly proportional to the temperature and mass of the disk, due to the fact that they (in most cases) sample the Rayleigh-Jeans tail of the spectral energy distribution (SED), and that the disk can be assumed to be optically thin at these wavelengths. At the same time, the thermal radiation in the submm is dominated by large and cool dust grains, thus providing a better estimate of the total dust mass (although still giving just a lower limit). By combining submm observations with IR-photometry a fit to the SED can be made, yielding constraints on the temperature and radial extent of spatially unresolved disks.

In this paper we present the first results of a Large Programme submm-survey with the *Large APEX Bolometer CAmera* (LABOCA) at the *Atacama Pathfinder EXperiment* (APEX) telescope, targeting stars of spectral type B to M, typically belonging to nearby stellar associations with ages ranging between 10 and 100 Myr. While the main aim of the study is to investigate disk evolution by relating disk parameters and grain properties to fundamental stellar parameters (metallicity, mass, and age), we also hope to spatially resolve extended dust disks around some of the most nearby stars. The observational scheme is designed to reach ~2 mJy/beam root-mean-square (RMS) sensitivity, enabling the detection of debris disk masses as low as the mass of the Moon (comparable to the Solar System's Kuiper-belt mass of 3 $M_{\rm Moon}$; Iorio 2007, and references therein), and to make observations of exo-Kuiper-belts out to distances of about 50−100 pc. A successful precursor study of the ~12 Myr-old β Pictoris Moving Group clearly detected 2 out of 7 stars (Nilsson et al. 2009).

2. Stellar sample

The sample of 22 F-, G-, and K-type stars selected for this first round of observations were based on levels of far-IR excess (measured by *IRAS*, *ISO* and *Spitzer*) and proximity (also making them targets for *Herschel Space Observatory* Key Programmes on debris disks), in order to optimise initial detection rates and get meaningful upper limits. Positions, spectral types, ages, and distances of the objects are listed in Table 1, together with integration times of the observations. The age estimates of most stars, which are based on lithium abundances, H-R diagram location, moving group (MG) association, chromospheric activity, etc., all carry large uncertainties. E.g., HD 105 is a member of the Tuc-Hor MG (Mamajek et al. 2004), with an estimated age of 27 ± 11 Myr (Mentuch et al. 2008), but could be as old as 225 Myr based on the level of chromospheric activity (Apai et al. 2008); and HD 98800, HD 25457, HD 141569, HD 152404, and HD 207129 might still be in their pre-main-sequence phase. Due to these inconsistencies we have adopted probable approximate ages with upper and lower limits that encompass the range of published values from different methods. Consequently, our ability to resolve details about the temporal evolution of disk properties in the young 10−100 Myr systems, where terrestrial planet formation could still be in progress, according to, e.g., isotopic dating of meteorites and the Earth-Moon system (Touboul et al. 2007) and dynamical modelling (Mandell et al. 2007), is somewhat restricted.

3. Observations and data reduction

The 12-m diameter submm telescope APEX (Güsten et al. 2006) is located at an altitude of 5100 m in the Chilean Andes, offering excellent atmospheric transparency. It is operated jointly by Onsala Space Observatory, the Max-Planck-Institut für Radioastronomie, and the European Southern Observatory. Since 2007, the LABOCA bolometer array has been available for observations at a central wavelength of 870 μm (345 GHz) and bandwidth of 150 μm (60 GHz), covering a 11.′4 field-of-view with its array of 295 bolometers; each with a nearly circular 19.″2 full-width at half-maximum (*FWHM*) Gaussian beam (Siringo et al. 2009). A spiral pattern mapping mode was employed in order to recover fully sampled maps from the undersampled bolometer array. Siringo et al. (2009) provide a detailed description of the instrument, observing modes, performance and sensitivity.

Observations of the targets presented in Table 1 were obtained between June 4 and October 22, 2008, amounting to roughly 80 out of 200 allocated hours of this Large Programme. Several individual 7.5 min long spiral scans, producing raw maps with an approximately uniform noise distribution within a radius of about 4′ around the central position of the source, were obtained for each star. In-between these scans, skydips (to determine the correction for the atmospheric opacity), flux calibration, and measurements of pointing accuracy and focussing were performed on selected calibration objects.

The scans were reduced and combined using MiniCRUSH (v1.05), an adapted version of CRUSH (Comprehensive Reduction Utility for SHARC-2, Kovács 2008), with further processing for analysis and plotting of final maps in Matlab (v7.9.0). As all of the sources were relatively faint we used filtering and settings optimised for point source extraction, with full beam smoothing, resulting in clean maps with 27″ effective resolution. Details of the data reduction procedure can be found in Kovács (2008) and are summarised in Nilsson et al. (2009). The general reduction steps involve flux calibration (opacity correction and counts-to-Jy conversion), flagging of bad (unresponsive, very noisy, or those that were too fast or too slow) channels, correlated noise removal, despiking, data weighting, and map making. Siringo et al. (2009) can be consulted for a description of these steps and their relation to the observing mode of the instrument.

Table 1. Observing log with stellar properties and integration times.

Object ID	Name	RA[a] (h m s)	Dec. (° ′ ″)	Spectral type[b]	Age$^{\text{upper}}_{\text{lower}}$ (Myr)	Reference	Distance[c] (pc)	Integration time (min)
HD 105		00 05 52.54	−51 45 11.0	G0V	30^{3500}_{27}	1, 2, 27	40	104
HD 17390		02 46 45.10	−21 38 22.3	F3IV/V	$300^{800}_{?}$	3, 4	45	24
HD 21997		03 31 53.65	−25 36 50.9	A3IV/V	50^{150}_{200}	5, 3, 6	74	52
HD 25457		04 02 36.74	−00 16 08.1	F5V[d]	50^{150}_{30}	7	19	97
HD 30447		04 46 49.53	−26 18 08.8	F3V	20^{100}_{10}	6, 8	78	65
HD 31392		04 54 04.21	−35 24 16.3	K0V	1300^{4000}_{400}	9	26	53
HD 32297		05 02 27.44	+07 27 39.7	A0V	30^{50}_{20}	10	112	39
HD 61005		07 35 47.46	−32 12 14.0	G8V	180^{320}_{100}	11	35	53
HD 78702		09 09 04.21	−18 19 42.8	A0/A1V	220^{320}_{80}	6	80	91
HD 95086		10 57 03.02	−68 40 02.4	A8III	20^{50}_{15}	12, 13, 14	92	32
HD 98800	TV Crt	11 22 05.29	−24 46 39.8	K5V+K7V+M1V+?[e]	10^{20}_{3}	15	47	62
HD 109573	HR 4796	12 36 01.03	−39 52 10.22	A0V+M2.5[f]	10^{20}_{4}	16, 17, 18	67	185
HD 131835		14 56 54.47	−35 41 43.6	A2IV	14^{18}_{10}	8, 6	111	145
HD 139664		15 41 11.38	−44 39 40.3	F4V	200^{300}_{150}	7	18	170
HD 141569		15 49 57.75	−03 55 16.4	A0Ve+M2+M4[g]	5^{8}_{2}	19, 26	99	206
HD 152404	AK Sco	16 54 44.85	−36 53 18.6	F5V+F5V[h]	17^{18}_{16}	20	145	127
HD 161868	γ Oph	17 47 53.56	+02 42 26.2	A0V	180^{190}_{170}	16, 17	29	218
HD 164249		18 03 03.41	−51 38 56.4	F5V	12^{20}_{8}	21	47	166
HD 170773		18 33 00.92	−39 53 31.3	F5V	200^{300}_{150}	3, 5	36	311
HD 193307		20 21 41.03	−49 59 57.9	G0V	5700^{6300}_{5100}	22, 27	32	90
HD 195627		20 35 34.85	−60 34 54.3	F0V	30^{230}_{10}	3, 12	28	98
HD 207129		21 48 15.75	−47 18 13.0	G2V	3000^{8000}_{10}	5, 22, 24, 25, 27	16	354

Notes. [(a)] Positions are from the Hipparcos Catalogue (Perryman et al. 1997). [(b)] Spectral types are from Torres et al. (2006); Thorén & Feltzing (2000); Manoj et al. (2006); Thévenin & Idiart (1999). [(c)] Distances are from the Hipparcos Catalogue (Perryman et al. 1997) [(d)] From López-Santiago et al. (2006). Marked as T Tau-type in SIMBAD astronomical database. [(e)] Quadruple system composed of two spectroscopic binaries, Aa+b and Ba+b, separated by 0.″848 (Prato et al. 2001). IR excess originates from the Ba+b (K7+M1V binary) component (for which the coordinates are given) (see Laskar et al. 2009, and references therein). [(f)] Binary system with the secondary (M2.5 pre-main-sequence) star located 7.″7 to the southwest of the primary (A0V). IR excess comes from HD 109573A (also designated HR 4796A or GQ Lup) with an imaged circumstellar ring (Schneider et al. 2009). [(g)] Primary component HD 141569A, which is possibly still in its pre-main-sequence stage, has a binary companion consisting of two M stars at ∼ 8″ separation. The double pair could be unbound and merely flying by (Reche et al. 2009). [(h)] Spectroscopic binary with high IR excess attributed to long-lived primordial, circumbinary disk (Uzpen et al. 2007; Gómez de Castro 2009).

References. (1) Hollenbach et al. (2005) and references therein; (2) Apai et al. (2008); (3) Zuckerman & Song (2004b); (4) Zuckerman & Song (2004a); (5) Song et al. (2003); (6) Moór et al. (2006); (7) López-Santiago et al. (2006) and references therein; (8) Rhee et al. (2007) and references therein; (9) Carpenter et al. (2009) and references therein; (10) Perryman et al. (1997); (11) Roccatagliata et al. (2009); (12) Lowrance et al. (2000); (13) de Zeeuw et al. (1999); (14) Mamajek et al. (2002); (15) Barrado Y Navascués (2006); (16) Song et al. (2001); (17) Rieke et al. (2005); (18) Stauffer et al. (1995); (19) Weinberger et al. (2000); (20) Chen et al. (2005) and references therein; (21) Zuckerman et al. (2001); (22) Mamajek & Hillenbrand (2008); (23) Henry et al. (1996); (24) Bryden et al. (2006) and references therein; (25) Zuckerman & Webb (2000); (26) Merín et al. (2004); (27) Valenti & Fischer (2005).

The final maps had a sensitivity between 2 and 10 mJy/beam. The integrated flux density of detected sources was found by fitting a 2-D Gaussian to the source region after baseline subtraction and gradient correction, with errors estimated from root-mean-square (RMS) noise calculation in the specific integration region, together with an absolute calibration error estimated to be 10% (Siringo et al. 2009).

4. Results

Of the 22 far-IR excess stars observed, 10 (HD 21997, HD 95086, HD 98800, HD 109573, HD 131835, HD 141569, HD 152404, HD 161868, HD 170773, and HD 207129) were detected with at least a 3σ significance, giving a detection rate of ∼45%. Five of the debris disks (HD 95086, HD 131835, HD 161868, HD 170773, and HD 207129) have previously never been seen at submm wavelengths. HD 105, HD 30447, and HD 195627 are listed as marginally detected in Table 2, showing flux peaks of >2.5σ significance at the position of the star.

The final 870 μm flux-density maps of the detected and marginally detected objects are found in Fig. 1, which show the flux level colour-coded in a scale ranging from zero to the peak flux density (in Jy/beam) of each individual map. The dotted contour represents the 1σ-level and the first solid contour outlines the 2σ-level, with subsequent contour lines spaced by 1σ. A circle representing the effective 27″ beam size after smoothing, and a line showing the angular size subtended by 1000 AU at the distance of the object, has been inserted in the lower left corner.

Several significant flux density peaks can be found surrounding the position of the observed star, also in parts of the LABOCA field-of-view outside the plotted 200 × 200″ maps. Considering the (down to) 2 mJy/beam sensitivity we are expected to hit the extragalactic confusion limit, permitting

Table 2. Integrated flux density, root-mean-square noise levels, and derived dust temperature, power-law exponent of the opacity law, mass, fractional dust luminosity, and characteristic radial dust distances for the 22 stars observed at 870-μm.

Object ID	Integrated flux sensity, F (mJy)	RMS noise, σ (mJy/beam)	$T_{\rm dust}$[a] (K)	β	Dust mass[b], $M_{\rm dust}$ ($M_{\rm Moon}$)	$f_{\rm dust}$ (10^{-4})	$R_{\rm dust}$ (AU)
DETECTIONS (>3σ)							
HD 21997	17.6 ± 8.0	4.6	52	0.7	33 ± 15	4.9	240
HD 95086	41.3 ± 18.4	10.4	150+(15−45)[c]	...	>76[d]	6.4−14	16+(250−1500)
HD 98800	33.6 ± 8.4	3.9	155[e]	0.1	8.5	470	2.4
HD 109573	21.5 ± 6.6	3.1	88[f]	0.7	19.5 ± 6.0	38	77
HD 131835	8.5 ± 4.4	3.0	89	0.1	21 ± 11	25	47
HD 141569	12.6 ± 4.6	2.3	80[g]	0.8	27 ± 10	73	110
HD 152404	42.9 ± 9.8	3.7	...[h]	...	...	...	...
HD 161868	12.8 ± 5.2	2.5	73	0.5	2.6 ± 1.1	0.90	120
HD 170773	18.0 ± 5.4	2.6	43	0.7	9.7 ± 2.9	4.5	170
HD 207129	5.1 ± 2.7	2.1	38	0.7	0.6 ± 0.3	0.94	130
MARGINAL DETECTIONS (>2.5σ)							
HD 105	10.7 ± 5.9	3.7	40	0.6	7.7 ± 4.2	2.6	110
HD 30447	6.9 ± 5.0	4.5	61	0.3	12.3 ± 8.9	9.3	56
HD 195627	13.0 ± 7.1	4.1	57	0.3	3.1 ± 1.7	1.0	74
NON-DETECTIONS							
HD 17390	...	6.8	55[i]	...	<13.4	1.9[j]	...
HD 25457	...	3.3	70[k]	...	<0.9	1.0[k]	...
HD 31392	...	4.7	49[k]	...	<3.4	1.6[k]	...
HD 32297	...	6.5	30[l]	...	<150	33[j]	...
HD 61005	...	6.0	58[k]	...	<6.6	25[k]	...
HD 78702	...	4.2	36[m]	2.0[m]	<39	2.6[m]	...
HD 139664	...	3.5	78[n]	...	<0.7	1.2[n]	...
HD 164249	...	3.5	78	...	<5.3	5.9[o]	...
HD 193307[p]	...	3.8	...	...	...	...	...

Notes. [a] For detected and marginally detected sources we use the dust temperature derived from the best fit to the spectral energy distribution. [b] Upper 3σ limit on the dust mass for undetected sources. [c] In order not to be resolved the second dust belt should be at <1500 AU, which would mean >15 K, while a temperature >45 K would not be compatible with far-IR data. [d] Calculated for upper limit on dust temperature. [e] Ambiguous fit (see discussion in Sect. 5.2). [f] Source appears spatially resolved (see discussion in Appendix A). See also more detailed modelling by Augereau et al. (1999b) and SCUBA measurement by Sheret et al. (2004). [g] Source appears spatially resolved (see discussion in Appendix A). See also modelling by Sheret et al. (2004). [h] No simple debris disk model can be fitted (see Section 5.2). [i] From Rhee et al. (2007). [j] From Moór et al. (2006). [k] From Hillenbrand et al. (2008). [l] From Maness et al. (2008). [m] From Williams & Andrews (2006). [n] From Beichman et al. (2006a). [o] From Rebull et al. (2008). [p] Not enough photometry data for reliable SED fit.

detection of many background submm galaxies (see e.g., Wang et al. 2004). This also effects the interpretation of our results for HD 109573 and HD 141569, which appear spatially resolved even with our rather large effective beam which had been optimised for point source extraction in the reductions. These issues are discussed further in Appendix A.

The measured integrated fluxes and RMS noise levels are listed in Table 2, together with the disk parameters (temperature, power-law exponent of the opacity law, dust mass, fractional dust luminosity, and characteristic radial distance of the dust) derived from the analysis outlined in Sect. 5. For undetected sources, an upper 3σ limit on the dust mass is given.

5. Discussion

5.1. Frequency of cold dust disks

Similar to the results of Carpenter et al. (2005), we find that about half of the stars previously observed to have far-IR fluxes in excess of stellar photospheric flux also have an excess of submm continuum emission. The five new submm disks discovered increase the number of known exo-Kuiper-belt systems from 29 to 34 (see Appendix B), counting the possible transitional disks[1] (HD 98800, HD 141569, HD 152404), and with three additional sources (HD 105, HD 30447, and HD 195627) awaiting confirmation. Although it is hard to estimate the total frequency of cold extended disks around main-sequence stars, it is likely to be at least the estimate of 10−15% suggested from *IRAS* (e.g. Backman & Paresce 1993; Rhee et al. 2007) and *Spitzer* (Hillenbrand et al. 2008) detections of debris disks around main-sequence stars, and may be up to 25% including disks too faint or cold to have been detected with current instrument sensitivities (Matthews et al. 2007).

An interesting result is that all four multiple systems in our sample, HD 98800, HD 109573, HD 141569, and HD 152404, were detected at 870 μm. Multiple stars have previously been deliberately left out from most debris disk surveys under the assumption that the formation of planetesimals in such systems would be inhibited. However, the *Spitzer* MIPS observations presented by Trilling et al. (2007) show that the incidence of debris disks around main-sequence A3−F8 wide (>50 AU) binaries is

[1] HD 98800, HD 141569, and HD 152404 are, according to spectroscopic studies by e.g. Furlan et al. (2007), Merín et al. (2004), and Alencar et al. (2003), respectively, pre-main-sequence stars and probably do not possess actual debris disks in the sense that they contain a large amount of gas, and might thus fall within the loosely defined transition disk category.

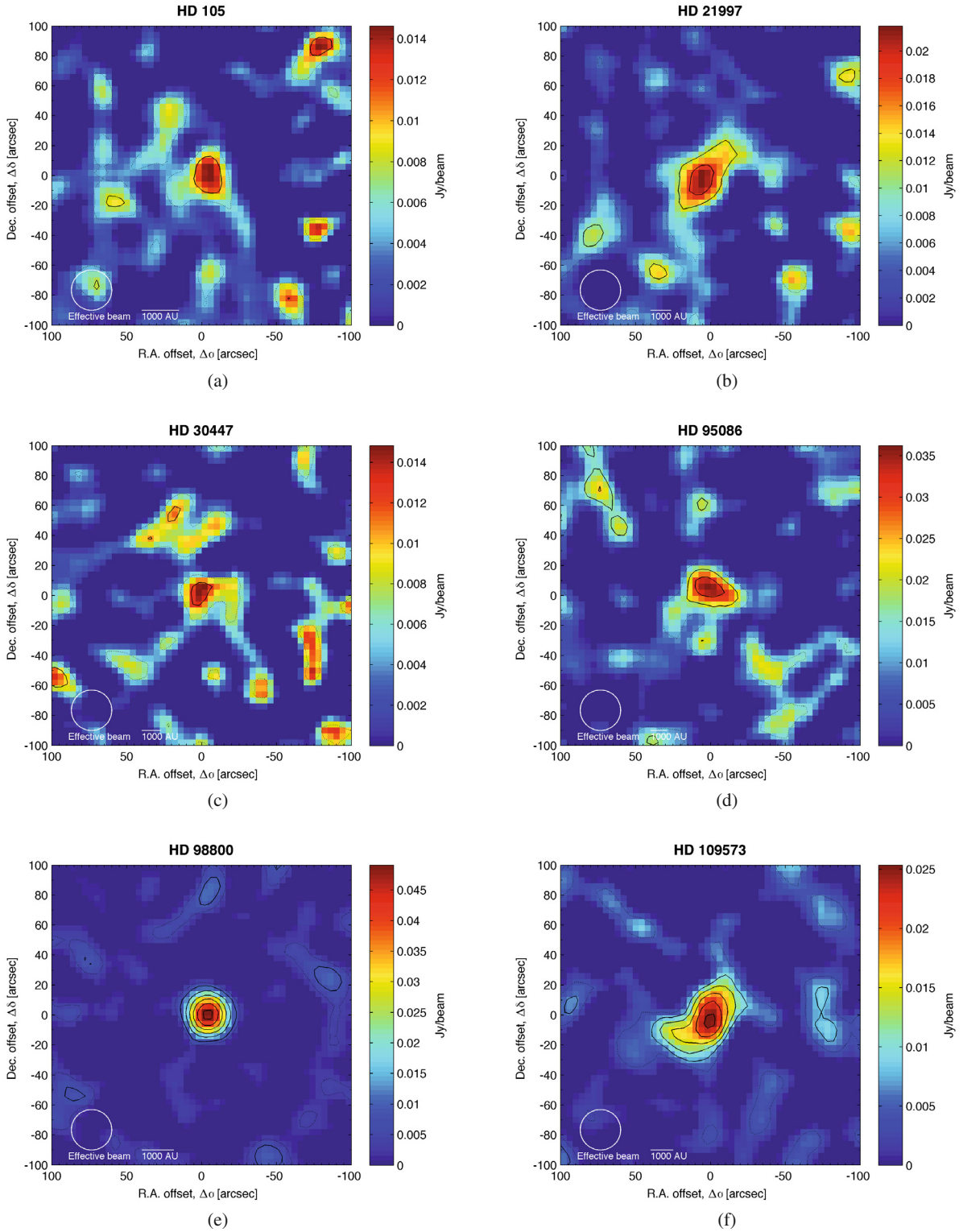

Fig. 1. Maps of objects detected at 870 μm with LABOCA at the APEX telescope. Each map has been smoothed with a circular Gaussian corresponding to the *FWHM* of the beam, and the resulting effective *FWHM* image resolution of 27″ is shown as a circle in the maps. In addition, a scale bar corresponding to 1000 AU at the distance of the star is inserted. The first solid contour represents 2σ flux levels, with the following contours at increments of 1σ (or 2σ for HD 98800 and HD 152404), while the dotted contour outlines the 1σ level. The position of the star is at $(\Delta\alpha, \Delta\delta) = (0'', 0'')$.

comparable to that around single stars and is even marginally higher for tight (<3 AU separation) binaries. Our results confirm these trends, since the four multiple star systems in our sample are three wide binaries and one spectroscopic tight binary (HD 152404). These results should however be taken with caution because of the morphological states of these four multiple

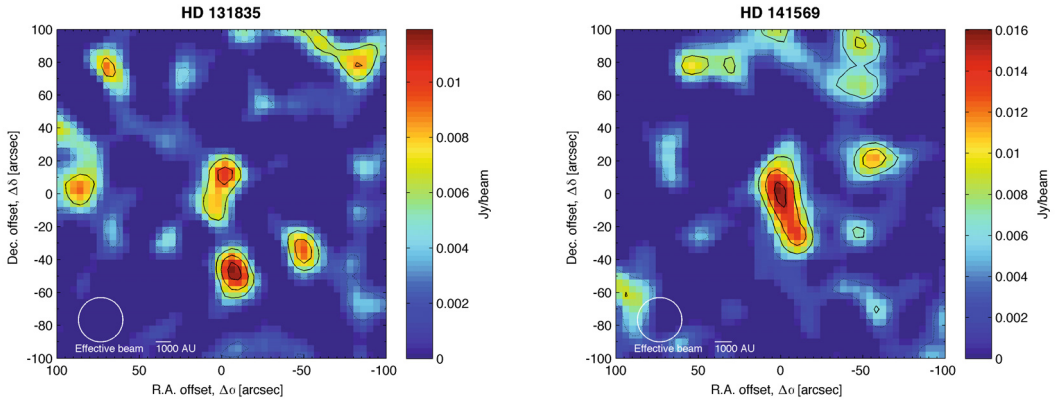

(g)

(h)

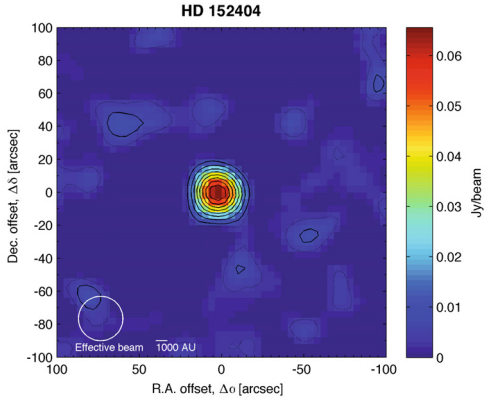

(i)

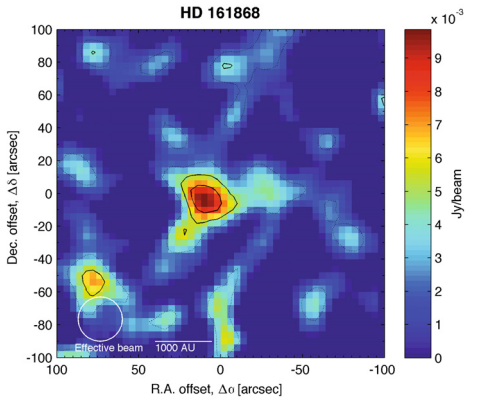

(j)

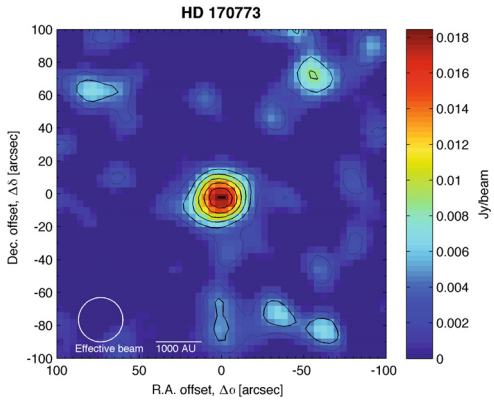

(k)

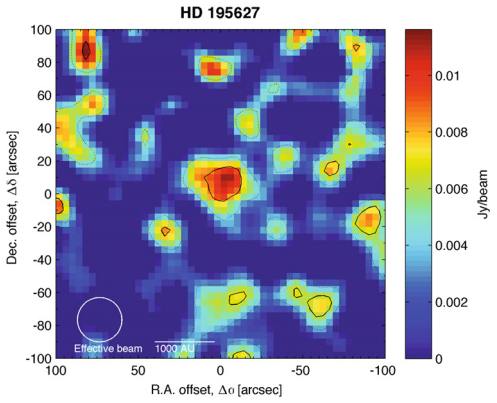

(l)

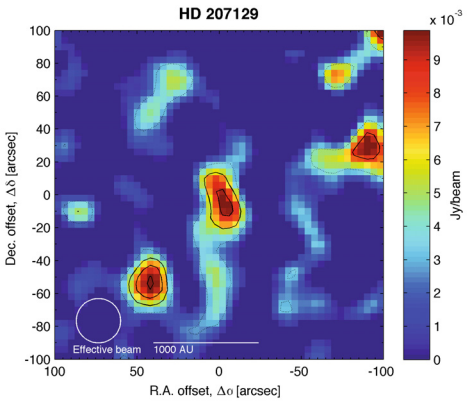

(m)

Fig. 1. continued.

stars systems. The main one is that all four systems are young (∼5−15 Myr old) and thus should naturally have a higher probability of possessing massive debris disks (see discussion in Sect. 5.5). This bias towards young stars in our sample of multiple star systems make it difficult to infer trends related to the binarity.

The fraction of detected debris disks in this first round of observations (45%) is considerably higher than that of previous submm surveys, e.g. that of nearby bright stars (9%, Holmes et al. 2003), β Pictoris Moving Group (17%, Nilsson et al. 2009; Liu et al. 2004), FEPS nearby stars (3%, Carpenter et al. 2005), nearby G stars (15%, Greaves et al. 2005), and M dwarfs (6%, Lestrade et al. 2006). This cannot only be explained by higher instrument sensitivity but is most likely due to a selection effect, having chosen an initial sample of stars with high far-IR excesses, and we are not expecting such a high detection rate from our ongoing Large Programme observations.

As anticipated with RMS noise levels as low as 2 mJy/beam we find a number of significant flux density peaks originating from background submm galaxies. Based on results from previous deep galaxy surveys at mm and submm wavelengths (e.g. Weiß et al. 2009; Bertoldi et al. 2007; Ivison et al. 2007; Clements et al. 2004) we would expect about 4−6 extragalactic sources to be detected (at $>3\sigma$ levels) in the LABOCA field-of-view with this sensitivity. This is consistent with the average number of four 3σ peaks within a 4′ radius around the central position of the source that we observe in our final maps. We can estimate the probability of a finding a random background source within an angular distance r of a given position from the expression $P(<r) = 1 - \exp(\pi\rho r^2)$ (Condon et al. 1998), where ρ is the source density per square degree. With a 27″ effective beam we calculate a roughly 2% likelihood of a chance alignment. Although the risk of a background galaxy falling within the central beam is so low, the probability that it does must be considered, as it could produce a false disk detection or a seemingly extended disk. With the commissioning of the *Atacama Large Millimetre/Submillimetre Array* (ALMA) now on its way, unprecedented angular resolution (≳0.″01, Peck & Beasley 2008) at submm and mm wavelengths (from 350 μm to 10 mm) will soon permit such ambiguities to be resolved.

5.2. Spectral energy distributions

By combining the integrated submm flux of our detected objects with photometry from optical and infrared measurements found in the literature, we made fits to the SED in order to find the dust temperature and radial extent of the disk. The star is modelled as a simple scaled blackbody, while the disk is approximated with a modified scaled blackbody function, as

$$F_{\rm disk}(\nu) = \frac{2h\nu^3}{\left(\exp\left(\frac{h\nu}{kT_{\rm dust}}\right)-1\right)c^2}\left(\frac{\nu}{\nu_0}\right)^{\beta}\kappa_0\Omega = \frac{\nu^{3+\beta}}{\left(\exp\left(\frac{h\nu}{kT_{\rm dust}}\right)-1\right)}C, \quad (1)$$

where h is Planck's constant, k is the Boltzmann constant, and c is the speed of light, with the radiating surface area and distance incorporated in the scale factor C. Here we assume that the opacity index varies with the frequency as a power law, i.e. $\kappa_\nu = \kappa_0(\nu/\nu_0)^\beta$, and that the grains dominating the flux in the IR and submm all have the same temperature. The latter simplifying assumption is applied since we do not have a spatially resolved source at submm wavelengths, although it would be reasonable to believe that colder dust located at Kuiper-belt distances would be responsible for most of the submm emission, while warmer dust located at asteroid-belt distances would dominate in the far-IR. Best-fit parameters were found by minimizing the reduced χ^2, i.e. the sum of squared errors weighted with the accuracy of the individual photometry measurements, divided by the number of degrees of freedom. Resulting SED fits are presented in Fig. 2, while values of the dust temperature, $T_{\rm dust}$, and the power law exponent of the opacity law, β, for the 10 detected (and 3 marginally detected) objects are listed in Table 2.

Although only the best-fit β parameter is quoted (without errors), we note that in almost all fits a value between 0.2 and 0.7 gives roughly the same χ^2. The difficulty in determining β is due to relatively large errors in measured submm (and longer wavelength) data, in addition to the possible existence of colder dust that would have been better modelled with a second dust component, but now instead shifts β in a single component fit towards zero. One example is HD 95086 which clearly cannot be modelled with a single component dust disk. For this star we added a second disk with a lower temperature limited by the maximum extent of the unresolved disk (≲1500 AU) and upper limit constrained by the two IR points at 13 and 33 μm (Chen et al. 2006). The fit shown in Fig. 2(e) is for a lower limit 15 K disk. Overall, the derived β values for our sources indicate significantly larger (and perhaps amorphous and/or fractal) dust grains (Miyake & Nakagawa 1993; Mannings & Emerson 1994; Pollack et al. 1994) in circumstellar debris disks compared to the mostly unprocessed grains in the interstellar medium (ISM), which have $\beta \sim 2$ (Hildebrand 1983; Li & Draine 2001). This is in agreement with previous results by e.g. Najita & Williams (2005), Nilsson et al. (2009), and Roccatagliata et al. (2009) who found $\beta = 0-1$ for various debris disks.

In three cases the SED modelling does not yield a good fit. For the quadruple system HD 98800 (Fig. 2(e)) previous submm and mm photometry has produced somewhat differing results, viz. the 1350 μm flux from Sylvester et al. (2001) is significantly higher than the 1300 μm flux from Sylvester et al. (1996), with our 870 μm measurement more consistent with the latter for a typical Rayleigh-Jeans slope. It can not be excluded that processes related to the orbital phase of the tight (1 AU) binary HD 98800B cause this seemingly bimodal flux variation of its circumbinary disk. Photometric variability has been found at shorter wavelengths (Soderblom et al. 1998). In any case, this unusual system of two eccentric binaries orbiting each other with highly inclined orbital planes (see e.g. Verrier & Evans 2008, and references therein) should have a complicated dynamical effect on the debris (or transitional) disk around the B pair, e.g. the high IR-excess has been proposed to originate from a puffed up outer dust ring which is gravitationally perturbed by the HD 98800A binary at perihelion (50 AU) passage (Furlan et al. 2007).

For HD 141569 the mid-IR flux is difficult to fit consistently with longer wavelength data in a simple disk model, however our results are very similar to those of Sheret et al. (2004).

The photometry data of HD 152404 (AK Sco) can clearly not be fitted with a simple modified blackbody emitting disk. In Fig. 2(i) we have inserted a dashed line representing the SED of the binary consisting of two F5V stars, showing that excess emission is present already at $\lambda \lesssim 1$ μm. This is indicative of hot dust in the system's young circumbinary disk, and it is probably still in its protoplanetary or transitional disk stage.

Although more detailed modelling of the SED could have been performed (and for some sources previously has been made by other authors) the lack of sensitive photometry at wavelengths between ∼100−500 μm still hampers our ability to

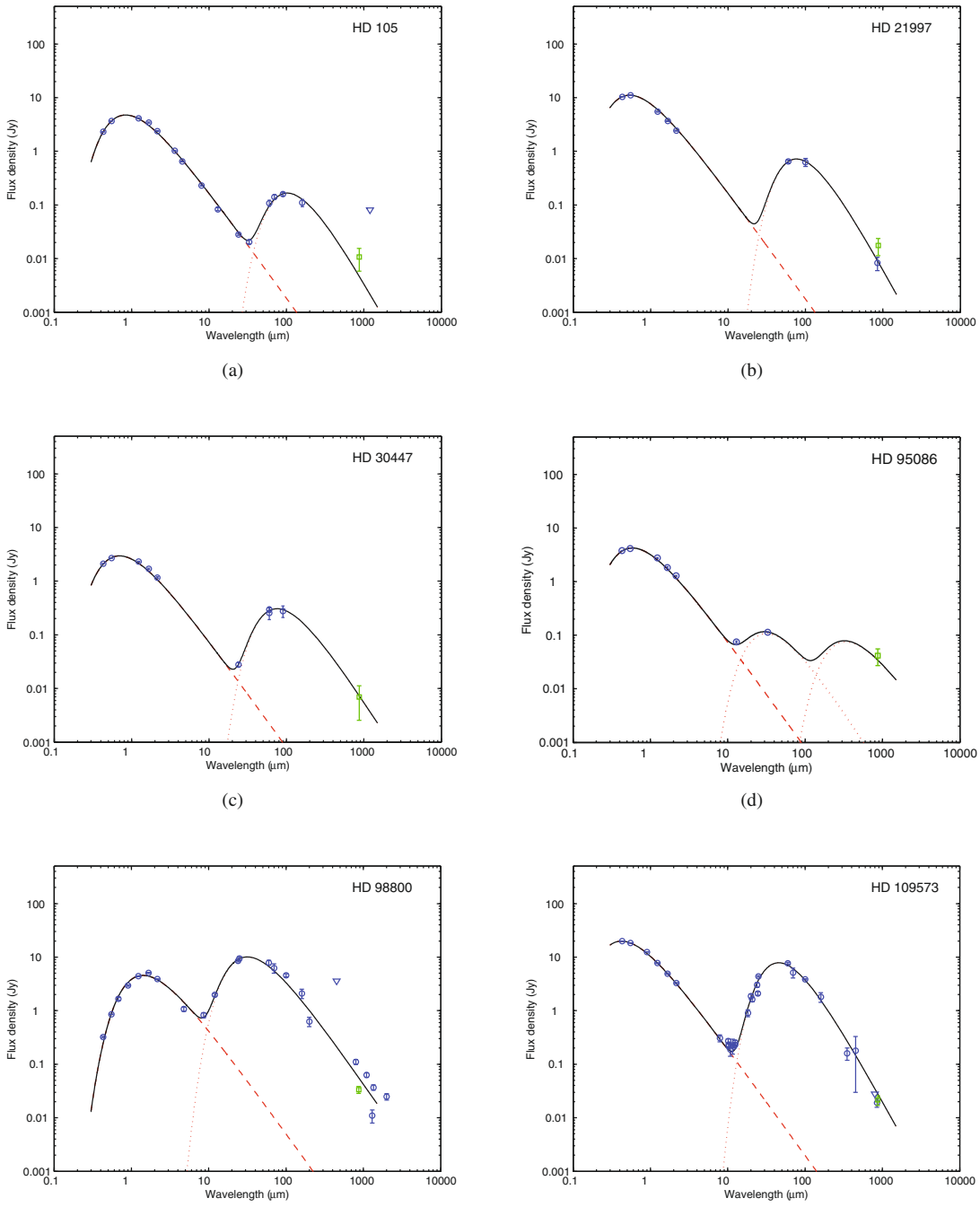

Fig. 2. The total modelled SEDs of detected objects are shown as a solid black line, with the stellar and disk components represented by red dashed and dotted lines, respectively. Our obtained 870 μm integrated flux density is given by a green square, while blue circular markers (and triangles symbolizing upper limits) are data from the literature. Fits which yield exceptionally high χ^2 values and other special cases are discussed in Sect. 5.2. The 800 μm flux measured for HD 141569 (red marker) at CSO (Walker & Butner 1995) has been left out of the fit since it is probably incorrect. REFERENCES: HD 105 (Moór et al. 2006; Hillenbrand et al. 2008; Carpenter et al. 2005; Cutri et al. 2003); HD 21997 (Moór et al. 2006; Williams & Andrews 2006; Cutri et al. 2003); HD 30447 (Moór et al. 2006; Cutri et al. 2003); HD 95086 (Chen et al. 2006; Cutri et al. 2003); HD 98800 (Low et al. 2005; Schütz et al. 2005; Mannings & Barlow 1998; Cutri et al. 2003; Walker & Heinrichsen 2000; Gregorio-Hetem et al. 1992; Garcia-Lario et al. 1990; Sylvester et al. 1996; Cieza 2008; Sylvester et al. 2001); HD 109573 (Moór et al. 2006; Sheret et al. 2004; Barrado Y Navascués 2006; Cutri et al. 2003; Low et al. 2005; Jura et al. 1995; Telesco et al. 2000; Jura et al. 1993; Fajardo-Acosta et al. 1998; Wahhaj et al. 2005); HD 131835 (Moór et al. 2006; Cutri et al. 2003); HD 141569 (Sylvester et al. 2001, 1996; Beichman et al. 1988; Walker & Butner 1995; Sheret et al. 2004); HD 152404 (Chen et al. 2005; Jensen et al. 1996; Acke et al. 2004; Cutri et al. 2003); HD 161868 (Su et al. 2008; Fajardo-Acosta et al. 1999; Jaschek et al. 1991; Cutri et al. 2003); HD 170773 (Moór et al. 2006; Cutri et al. 2003); HD 195627 (Rebull et al. 2008; Sylvester & Mannings 2000; Mannings & Barlow 1998; Cutri et al. 2003); HD 207129 (Mannings & Barlow 1998; Trilling et al. 2008; Schütz et al. 2005; Cutri et al. 2003; Mamajek et al. 2004; Laureijs et al. 2002; Jourdain de Muizon et al. 1999; Tanner et al. 2009).

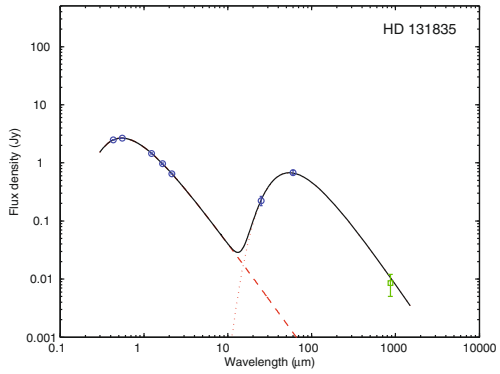

(g)

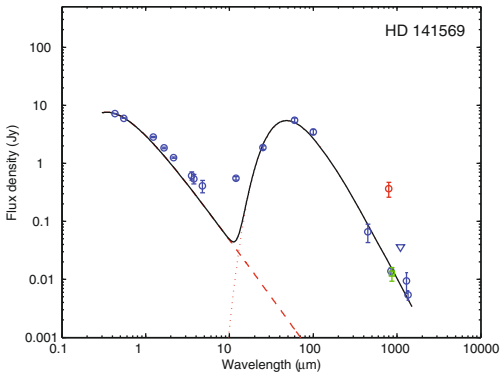

(h)

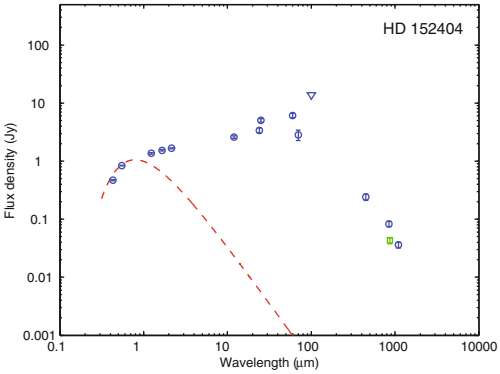

(i)

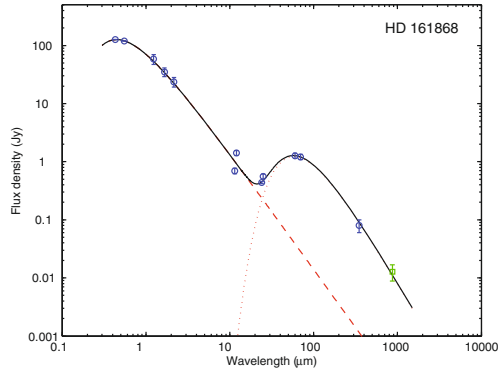

(j)

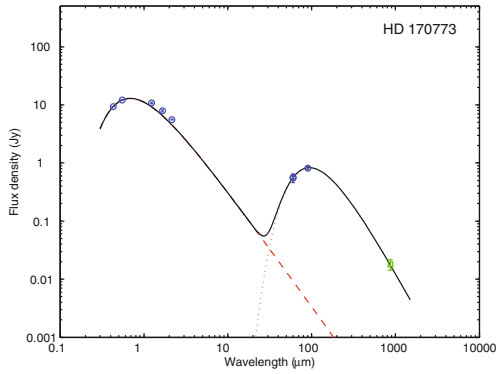

(k)

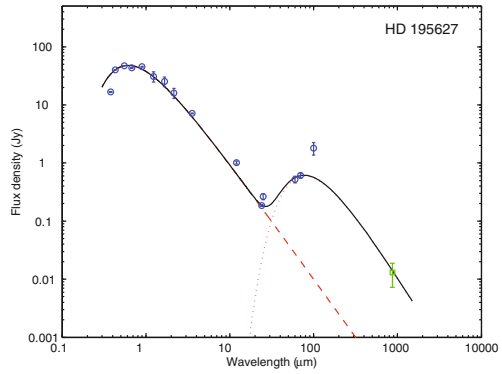

(l)

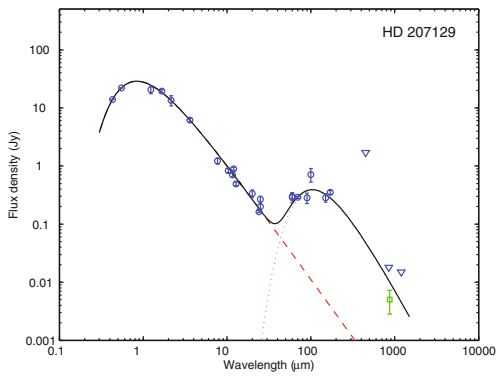

(m)

Fig. 2. continued.

accurately determine grain properties and size distributions in cold debris disks. This will be addressed with ongoing *Herschel* PACS/SPIRE observations of disks, which are filling the gap between current far-IR and submm measurements, and will detect dust masses down to a few Kuiper-belt masses for nearby stars (Danchi et al. 2010). With such data, any deviation from the theoretical power law size distribution of observable dust, e.g. the "wavy" size distribution predicted from numerical models of collisional processes in debris disks (Thébault & Augereau 2007; Krivov et al. 2006), can be thoroughly investigated. In addition, ALMA will enable detection and imaging of many faint disks, and permit detailed SED modelling of the very coldest Kuiper-belt systems.

5.3. Dust masses and characteristic radial distances

For an optically thin disk at submm wavelengths we can make an estimate of the mass of large and cool dust grains (which contain most of the dust mass), providing a lower limit on the total dust mass required to reproduce the measured flux (Hildebrand 1983):

$$M_{\rm dust} = \frac{F_\nu d^2}{\kappa_\nu B_\nu(T_{\rm dust})}, \tag{2}$$

where d is the distance to the source, and the integrated flux density F_ν at 870 μm is assumed to lie on the Rayleigh-Jeans tail of the SED, thus B_ν appropriately expressed as $B_\nu = 2\nu^2 kT/c^2$. The opacity (or dust mass absorption coefficient), κ_ν at submm wavelengths is currently unknown due to uncertainties in the composition and structure of dust grains, but based on results from Draine & Lee (1984) the 870 μm opacity for micron-sized spherical silicate grains should be $\sim$0.5 cm^2 g^{-1}, and approximately four times as high for graphite grains at a temperature of 100 K. Allowing for porous grains would significantly increase the opacity (see Stognienko et al. 1995, and references therein), but we adopt $\kappa_\nu = 2$ cm^2 g^{-1} (as in Liseau et al. 2003; Nilsson et al. 2009), similar to the commonly chosen 1.7 cm^2 g^{-1} (e.g. Zuckerman & Becklin 1993; Dent et al. 2000; Najita & Williams 2005). The distance d to the source and the derived dust temperature $T_{\rm dust}$ are two additional parameters with large errors that amplify the inaccuracy of the mass determination. Calculated $M_{\rm dust}$ is given in Table 2 with errors based only on the uncertainty in the integrated flux density.

In general, the estimated dust masses fall in the mass range of a few moon masses which is typical for submm detected debris disks at current sensitivities. One exception is HD 95086 with a dust mass in excess of 76 $M_{\rm Moon}$ assuming a second disk component at the upper 45 K temperature limit.

Another disk parameter that can be obtained from the best-fit $T_{\rm dust}$ and β is the characteristic radial dust distance $R_{\rm dust}$, which can be found by assuming thermal equilibrium of dust grains (see e.g. Emerson 1988), i.e. the emitted (modified blackbody) power

$$P_{\rm e} = 4\pi a^2 F_{\rm dust} = 8h\left(\frac{\pi a}{c}\right)^2\left(\frac{1}{\nu_0}\right)^\beta\left(\frac{kT_{\rm dust}}{h}\right)^{4+\beta}\int_0^\infty \frac{x^{3+\beta}}{{\rm e}^x-1}{\rm d}x \tag{3}$$

equals the absorbed power

$$P_{\rm a} = \frac{R_*^2\sigma T_{\rm e}^4}{R_{\rm dust}^2}\pi a^2\,(1-A)\,. \tag{4}$$

In Eq. (3) we made the variable substitution $x = (h\nu)/(kT_{\rm dust})$. The integral can be analytically expressed yielding a characteristic radial dust distance given by

$$R_{\rm dust} = \left(\frac{L_*\,(1-A)\,c^2\nu_0^\beta}{32\pi^2 h\,(kT_{\rm dust}/h)^{4+\beta}\,\zeta\,(4+\beta)\,\Gamma\,(4+\beta)}\right)^{1/2}, \tag{5}$$

where L_* is the luminosity of the star, and A is the albedo of the dust grains. $\zeta\,(s) = \Sigma_{n=1}^{\infty} n^{-s}$ is the Riemann zeta function and $\Gamma(n)$ is the Gamma function. Here we also have to assume a ν_0 and corresponding grain size a for which the adopted power-law dependence of the opacity is valid. According to the results from Draine & Lee (1984) the power-law relation holds for $\lambda_0 \lesssim 3\,\mu$m, and we choose $a = 1.0\,\mu$m in our calculation. The albedos of micron-sized dust grains are generally below 0.1, as shown by modelling (Shen et al. 2009) and observations of cometary and zodiacal dust (Lasue & Levasseur-Regourd 2006; Reach et al. 2003), thus we use $A = 0$, and note that an albedo of almost 0.20 would be required to reduce $R_{\rm dust}$ with 10%. The results are presented in the last column of Table 2. With the exception of HD 98800B, for which we derive a characteristic dust distance of $\sim$2 AU in accordance with e.g. Furlan et al. (2007); Akeson et al. (2007); Prato et al. (2001) and consistent with the smallest stable circumbinary orbit (Holman & Wiegert 1999), all detected disks have $R_{\rm dust}$ comparable to Kuiper-belt distances or beyond.

The inferred sizes of the detected disks is also a reason for hesitation in regarding the extended flux density distribution around HD 109573 and HD 141569 as resolved disks (see further discussion in Appendix A). At distances of 67 pc and 99 pc, and sizes of 77 AU and 110 AU, respectively, their angular size in comparison with some other disks (e.g. the 170 AU disk around HD 170773, 36 AU away) would be smaller (assuming similar grain properties and size distributions), suggesting these other disks should also have been resolved in our observations.

5.4. Fractional dust luminosities

Since stellar distances, dust opacities and temperature distributions are uncertain, the error in the determined $M_{\rm dust}$ is actually larger than the ones given in Table 2 (which was derived from measured flux-density errors), but difficult to quantify. A more independent estimate of the amount of dust in the system can be made by calculating the fractional dust luminosity, $f_{\rm dust} = L_{\rm dust}/L_*$, from the fitted SEDs. In Table 2 we have listed fractional dust luminosities found from our SED modelling of detected sources, and values from the literature for undetected sources. Again HD 98800 stands out, with an exceptionally high $f_{\rm dust}$, attributed to hot dust belts of the order of $\sim$1 AU from the binary HD 98800B (Furlan et al. 2007).

Since all observed stars are nearby the effects of interstellar extinction should be be negligible, which is also confirmed by $B-V$ colour excesses below $\sim$0.1. The only exception is again HD 152404 (which is however not modelled) with $E_{B-V} = 0.28$. This could be both due to its distance (145 pc) and its T Tauri nature. The general consequence of uncorrected reddening would be an overestimation of the fractional dust luminosity, and has to be checked for in sources outside the Local Bubble.

5.5. Temporal evolution of debris disks

Both theoretical and previous observational work have indicated that the amount of dust in debris disks, on the average, will decrease from $\sim$10 Myr as the disk ages. This is to be expected, due to the combined effect of collisional grinding producing

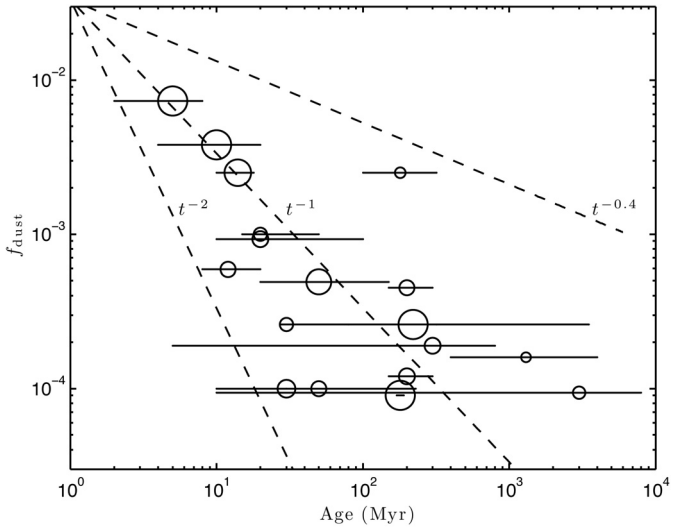

Fig. 3. Fractional dust luminosity plotted against stellar age for the observed sample of stars. For detected sources our derived values have been used, while values from the literature (where available) have been used for undetected ones (see references in Table 2). Age references are given in Table 1. The size of the circular markers represent the stellar spectral type (diameter increase linearly with earlier spectral type). Dashed lines have been inserted for comparison with the temporal evolution found from previous observations and models.

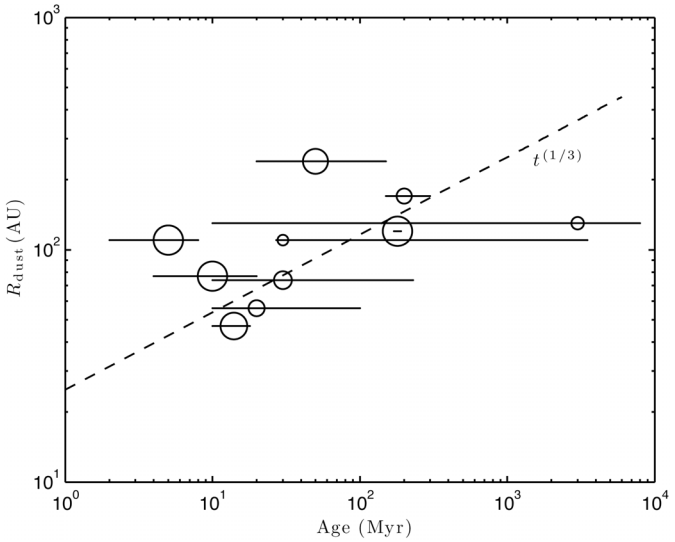

Fig. 4. Characteristic radial dust distance for detected submm disks plotted against stellar age. Age references can be found in Table 1. The dashed line shows the expected slope for the temporal evolution of dust in a planetesimal disks dominated by self-stirring (Kenyon & Bromley 2008, 2004).

small grains that are blown out by radiation pressure, Poynting-Robertson drag, sublimation and photosputtering of ices (e.g. Wyatt et al. 2007; Wyatt 2008), and is the general behaviour confirmed in debris disk surveys (e.g Najita & Williams 2005; Su et al. 2006). Spangler et al. (2001) found $f_{\rm dust} \propto t^{-\alpha}$ with $\alpha = 2$ from ISO observations of clusters, but these results were not confirmed by later studies that found significantly lower α, e.g. Liu et al. (2004) derived $\alpha = 0.5$–1.0 and Su et al. (2006) $\alpha = 0.6$, from *Spitzer* and JCMT observations, respectively. The main uncertainty lies in the inaccuracy of current age estimates of individual stars, as discussed in Sect. 2, and possible variations in disk evolution depending on stellar spectral types. Nilsson et al. (2009) compared the average fractional dust luminosity observed in the ~12 Myr β Pictoris Moving Group with the ~100 Myr Pleiades cluster (Greaves et al. 2009) and obtained $\alpha > 0.8$. Interestingly, these values are higher than those predicted from models of collisional dust evolution, which predict a slower decline, with α as low as 0.4 (Wyatt et al. 2007; Löhne et al. 2008). In Fig. 3 we have plotted $f_{\rm dust}$ versus age for the observed sample of stars in this study, with the diameter of the circular marker scaled linearly with stellar spectral type (increasing for earlier spectral types). Due to the large age uncertainties (represented by horizontal error bars) we refrain from making a fit, and instead only display dashed lines showing the expected decline for three different values of α. We conclude that the temporal evolution of the fractional dust luminosity determined from our observations is in agreement with Nilsson et al. (2009), and $f_{\rm dust}$ could perhaps decline as fast as the t^{-2} found by Spangler et al. (2001), although $\alpha < 0.8$ can not be excluded due to large error bars and small stellar sample. This trend will be better constrained after the completion of the ongoing APEX/LABOCA Large Programme.

Note that this issue is an important one because the value of α should be an indication of the dominant process for dust removal: $\alpha \geq 1$ values are in principle only possible for systems at steady-state where Poynting-Robertson drag dominates, while $\alpha \leq 1$ corresponds to collision dominated systems at steady state (Dominik & Decin 2003). However, the problem could be more complex if the collisional evolution of the system is controlled by self-stirring, triggered by the formation of large, 1000–2000 km sized embryos. In this case, the system can brighten from an early low state before later reaching the steady state collisional decline (Kenyon & Bromley 2008, 2004; Wyatt 2008). An interesting characteristic of self-stirred disks is that the peak of dust production, which coincides with the formation of planetary embryos, should be reached at different times depending on the radial distance to the star. This dust production peak should thus propagate outward with time, leading to a progressive increase of the observed characteristic dust distance $R_{\rm dust}$ with age as $t^{1/3}$. We have tried to identify this evolutionary trend by plotting $R_{\rm dust}$ of our detected submm disks versus age (in Fig. 4). In contrast to Najita & Williams (2005), who found no apparent correlation for a sample of 14 submm detected disks, we do identify an increase in characteristic radial dust distance with increasing age, although it is again difficult to make any firm conclusion regarding the power-law exponent. These tentative results will also have to be confirmed with additional detections in ongoing observations.

For both the fractional dust luminosity and the characteristic radial dust distance there seems to be no obvious dependence on stellar spectral type.

6. Conclusions

The most important results from our 870 μm observations of 22 exo-Kuiper-belt candidates can be summarised as follows:

- Out of the observed sample of far-IR excess stars we detected ~45% (10 out of 22) with at least a 3σ significance. Five of the detected debris disks (HD 95086, HD 131835, HD 161868, HD 170773, and HD 207129) have previously

never been seen at submm wavelengths. These findings increase the currently known exo-Kuiper-belts (inferred from cold extended dust disks detected in the submm) from 29 to 34. The sensitivity of current submm observations with LABOCA at APEX and SCUBA at JCMT are approaching the background extragalactic confusion limit, as is evident from the abundance of significant off-centre flux density peaks in acquired submm maps. Future ALMA observations will be essential to distinguish between resolved disks and background submm galaxies.

- We perform SED modelling of available photometric data using a simple modified blackbody to make a χ^2 minimisation fit to the disk excess emission in order to determine the dust temperature $T_{\rm dust}$ and power-law exponent β of the opacity law. Resulting β parameters are all between 0.1 and 0.8, suggesting grains significantly larger than those in the ISM, in agreement with previous results for debris disks (e.g. Najita & Williams 2005; Nilsson et al. 2009; Roccatagliata et al. 2009). However, it should be noted that the presence of colder secondary dust components in addition to the fitted disk could be responsible for some abnormally low β values. The measured 870 μm flux of HD 95086 undeniably requires a second disk component.
- Besides finding the dust mass of detected sources (together with upper limits on undetected ones) derived from the integrated 870 μm flux density, we use the best-fit SED parameters to calculate the fractional dust luminosity $f_{\rm dust}$ and the characteristic radial dust distance $R_{\rm dust}$ (for 1μm sized grains) of the disks. We present plots of the temporal evolution of $f_{\rm dust}$ and $R_{\rm dust}$ based on these values together with previously estimated stellar ages, and find that our results are consistent with a $f_{\rm dust} \propto t^{-\alpha}$, with $\alpha \sim 0.8{-}2.0$, as well as tentatively with the $R_{\rm dust} \propto t^{1/3}$ relation predicted in debris disks collisional evolution models by Kenyon & Bromley (2004).

Acknowledgements. This research was supported by financial contributions from Stockholm Astrobiology Graduate School, and the International Space Science Institute (ISSI) in Bern, Switzerland ("Exozodiacal Dust Disks and Darwin" working group, `http://www.issibern.ch/teams/exodust/`). A.B. was funded by the *Swedish National Space Board* (contract 84/08:1).

Appendix A: Spatially resolved disks or chance alignment of background galaxies?

Two sources appear spatially resolved in our 870 μm maps, both of them are multiple systems which have been previously imaged at shorter wavelengths. Here we compare the resolved structures at submm wavelengths with that observed in scattered optical light and IR emission, and discuss the indications for and against them actually being resolved disks. The position angle (PA) was found by fitting a 2-D Gaussian profile to the extended submm emission.

A.1. HD 109573 (HR 4796)

The highly inclined debris disk around HD 109573A (also known as HR 4796A) was first imaged in the mid-IR by Koerner et al. (1998) and Jayawardhana et al. (1998), followed by optical and near-IR coronagraphic imaging by Schneider et al. (1999, 2009). These observations revealed a 17 AU wide dust ring with ~70 AU radius surrounding the primary A0V star. In our map (Fig. 1(f)), the peak flux density of 19.1 ± 3.1 mJy/beam is centred on the position of the primary, with the secondary M2.5 star located 7.″7 (~2 pixels) to the southwest. Surprisingly, the PA is 129°, compared to 27° for the ring imaged by Schneider et al. (2009), i.e. a nearly orthogonally oriented extension. Although the accuracy of our determined PA is hard to estimate due to the influence of possible lower-sigma noise features, the flux distribution is undoubtedly extended in the southeast direction, maybe with a warp toward the East. The 3σ contour reaches ≳2000 AU projected radial distance on that side of the central star. However, a chance alignment with a bright background galaxy to the southeast is probable, for several reasons. Firstly, an outer disk orthogonally oriented to the inner one seems highly implausible or even unphysical. In addition, a data reduction employing only half-beam smoothing seem to imply a separate 3σ peak in the southeast flux extension. A second galaxy to explain the small northwest extension is conceivable, but it could also be a noise feature. The formal likelihood of a source falling within some 25″ distance from the star and making it appear extended is about 4%.

A.2. HD 141569

This triple system has been extensively studied since the *Hubble Space Telescope* (HST) discovery of a large disk surrounding the primary A0Ve star HD 141569A (Weinberger et al. 1999; Augereau et al. 1999a). The disk has been imaged in thermal mid-IR emission (Fisher et al. 2000), but up until now never resolved at longer wavelengths. We find a clear asymmetric elongation of the disk with PA of 10° to the southwest of the source-centred 10.3 ± 2.3 mJy/beam peak flux (Fig. 1(h)). This can be compared to the two most detailed studies of the disk structure so far, employing coronagraphic HST ACS and STIS observations, respectively (Clampin et al. 2003; Mouillet et al. 2001), which revealed an inner (≲175 AU) clearing surrounded by two ring-like structures – a thin (~50 AU) belt at ~200 AU and a wider (~100 AU) belt at ~350 AU – oriented with a semi-major axis roughly in the North-South direction and connected by faint spiral structures. Clampin et al. (2003) also found additional spiral arcs extending from the northeast (out to ~1200 AU) and the southwest (toward the binary HD 141569BC, located ~8″ northwest of HD 141569A. The reason for the highly asymmetric brightness distribution in the optical, with respect both to semi-major and semi-minor axis, could be a non-axisymmetric distribution of grains and/or anisotropic scattering by grains (Mouillet et al. 2001). Suspected gravitational perturbation by a massive body in the disk, and effects from the binary companion has been extensively studied by e.g. Augereau & Papaloizou (2004); Quillen et al. (2005); Wyatt (2005), while Ardila et al. (2005) and Reche et al. (2009) thoroughly investigated the case of a gravitationally unbound binary passing by (with and without planets in the disk), but did not manage to explain all observed features. It is possible that we are seeing a colder dust population on very eccentric orbits, perhaps shaped by the dynamical interaction with the binary (either in a flyby or a triple system scenario), however, dynamical modelling of such a scenario is beyond the scope of the present paper. The extreme brightness asymmetry with respect to the semi-minor axis, on the other hand, does not make us confident that the extended emission originates from the dust disk, and could instead be attributed to a background galaxy located southwest of HD 141569. Also in this case a re-reduction applying only half-beam smoothing seem to hint at a separate 3σ peak, only 8″ to the southeast of the star (which would be a 0.5% chance alignment).

Appendix B: List of submm detected exo-Kuiper-belts

Table B.1. Submm and mm photometry of all debris disks that have been detected at submm and longer wavelengths.

Star	Other name	λ (μm)	F_ν (Jy)	Reference
HD 105		870	10.7 ± 5.9[a]	1
HD 377		1200	4.0 ± 1.0	11
HD 8907		1200	3.2 ± 0.9	11
HD 14055	γ Tri	850	5.5 ± 1.8	3
HD 15115		850	4.9 ± 1.6	3
HD 17206	τ^1 Eri	1300	20.7 ± 3.9	6
HD 21997		870	8.3 ± 2.3	3
		870	17.6 ± 8.0	1
HD 22049	ϵ Eri	450	225 ± 10	12
		850	40.0 ± 1.5	12
		1300	24.2 ± 3.4	6
HD 30447		870	6.9 ± 5.0[a]	1
HD 32297		1300	5.1 ± 1.1	10
HD 38393		850	2.4 ± 1.0	12
HD 39060	β Pic	850	58.3 ± 6.5	4
		870	63.6 ± 6.7	2
		1200	24.3 ± 3.0	5
		1300	24.9 ± 2.6	6
HD 39944		1350	3.7 ± 0.9	14
HD 48682	56 Aur	850	5.5 ± 1.1	12
HD 61005		350	95 ± 12	11
HD 95086		870	41.3 ± 18.4	1
HD 98800[b]	TV Crt	870	33.6 ± 8.4	1
		1350	36.8 ± 4.2	14
		2000	24.8 ± 3.4	14
HD 104860		350	50.1 ± 9.3	11
		1200	4.4 ± 1.1	11
HD 107146		350	319 ± 6	11
		450	130 ± 40	7
		850	20 ± 4	7
HD 109085	η Cor	850	7.5 ± 1.2	12
HD 109573	HR 4796	450	180 ± 150	12
		850	19.1 ± 3.4	8, 12
		870	21.5 ± 6.6	1
HD 123160		850	13 ± 4.3	14
		1350	4.7 ± 0.9	14
HD 128167	σ Boo	850	6.2 ± 1.7	12
HD 131835		870	8.5 ± 4.4	1
HD 141569[b]		450	66 ± 23	12
		850	14 ± 1	12
		870	12.6 ± 4.6	1
		1300	9.39 ± 3.72	13
		1350	5.3 ± 1.1	14
HD 152404[b]	AK Sco	450	242 ± 32	15
		800	83 ± 9	15
		870	42.9 ± 9.8	1
		1100	36 ± 4	15
HD 161868	γ Oph	870	12.8 ± 5.2	1
HD 170773		870	18.0 ± 5.4	1
HD 172167	Vega	850	45.7 ± 5.4	4, 12
		1300	11.4 ± 1.7	16
HD 181327		870	51.7 ± 6.2	2
HD 191089		350	54 ± 15	11
HD 195627		870	13.0 ± 7.1[a]	1
HD 197481	AU Mic	850	14.4 ± 1.8	9
HD 207129		870	5.1 ± 2.7	1
HD 216956	Fomalhaut	450	595 ± 35	12
		850	97 ± 5	12
		850	81 ± 7.2	4
HD 218396	V342 Peg	850	10.3 ± 1.8	3
HIP 23200	V1005 Ori	850	4.8 ± 1.2	9

Notes. [(a)] Marginally detected. [(b)] Debris disk status disputed.
References. (1) This paper; (2) Nilsson et al. (2009); (3) Williams & Andrews (2006); (4) Holland et al. (1998); (5) Liseau et al. (2003); (6) Chini et al. (1991); (7) Williams et al. (2004); (8) Greaves et al. (2000); (9) Liu et al. (2004); (10) Maness et al. (2008); (11) Roccatagliata et al. (2009); (12) Sheret et al. (2004); (13) Walker & Butner (1995); (14) Sylvester et al. (2001); (15) Jensen et al. (1996); (16) Wilner et al. (2002).

References

Acke, B., van den Ancker, M. E., Dullemond, C. P., van Boekel, R., & Waters, L. B. F. M. 2004, A&A, 422, 621
Akeson, R. L., Rice, W. K. M., Boden, A. F., et al. 2007, ApJ, 670, 1240
Alencar, S. H. P., Melo, C. H. F., Dullemond, C. P., et al. 2003, A&A, 409, 1037
Apai, D., Janson, M., Moro-Martín, A., et al. 2008, ApJ, 672, 1196
Ardila, D. R., Lubow, S. H., Golimowski, D. A., et al. 2005, ApJ, 627, 986
Augereau, J. C., & Papaloizou, J. C. B. 2004, A&A, 414, 1153
Augereau, J. C., Lagrange, A. M., Mouillet, D., & Ménard, F. 1999a, A&A, 350, L51
Augereau, J. C., Lagrange, A. M., Mouillet, D., Papaloizou, J. C. B., & Grorod, P. A. 1999b, A&A, 348, 557
Aumann, H. H., Beichman, C. A., Gillett, F. C., et al. 1984, ApJ, 278, L23
Backman, D. E., & Paresce, F. 1993, in Protostars and Planets III, ed. E. H. Levy, & J. I. Lunine, 1253
Barrado Y Navascués, D. 2006, A&A, 459, 511
Beichman, C. A., Neugebauer, G., Habing, H. J., et al. 1988, in Infrared astronomical satellite (IRAS) catalogs and atlases, Explanatory supplement, ed. C. A. Beichman, G. Neugebauer, H. J. Habing, P. E. Clegg, & T. J. Chester, Vol. 1
Beichman, C. A., Bryden, G., Stapelfeldt, K. R., et al. 2006a, ApJ, 652, 1674
Beichman, C. A., Tanner, A., Bryden, G., et al. 2006b, ApJ, 639, 1166
Bertoldi, F., Carilli, C., Aravena, M., et al. 2007, ApJS, 172, 132
Bryden, G., Beichman, C. A., Trilling, D. E., et al. 2006, ApJ, 636, 1098
Carpenter, J. M., Wolf, S., Schreyer, K., Launhardt, R., & Henning, T. 2005, AJ, 129, 1049
Carpenter, J. M., Bouwman, J., Mamajek, E. E., et al. 2009, ApJS, 181, 197
Chen, C. H., Jura, M., Gordon, K. D., & Blaylock, M. 2005, ApJ, 623, 493
Chen, C. H., Sargent, B. A., Bohac, C., et al. 2006, ApJS, 166, 351
Chini, R., Kruegel, E., Kreysa, E., Shustov, B., & Tutukov, A. 1991, A&A, 252, 220
Cieza, L. A. 2008, in ed. A. Frebel, J. R. Maund, J. Shen, & M. H. Siegel, ASP Conf. Ser., 393, 35
Clampin, M., Krist, J. E., Ardila, D. R., et al. 2003, AJ, 126, 385
Clements, D., Eales, S., Wojciechowski, K., et al. 2004, MNRAS, 351, 447
Condon, J. J., Cotton, W. D., Greisen, E. W., et al. 1998, AJ, 115, 1693
Cutri, R. M., Skrutskie, M. F., van Dyk, S., et al. 2003, 2MASS All Sky Catalog of point sources
Danchi, W. C., Eiroa, C., & Herschel DUNES Team. 2010, in BAAS, 41, 399
de Zeeuw, P. T., Hoogerwerf, R., de Bruijne, J. H. J., Brown, A. G. A., & Blaauw, A. 1999, AJ, 117, 354
Dent, W. R. F., Walker, H. J., Holland, W. S., & Greaves, J. S. 2000, MNRAS, 314, 702
Dominik, C., & Decin, G. 2003, ApJ, 598, 626
Draine, B. T., & Lee, H. M. 1984, ApJ, 285, 89
Emerson, J. P. 1988, in Formation and Evolution of Low Mass Stars, ed. A. K. Dupree, & M. T. V. T. Lago (Kluwer Acad. Publish.), 21
Fajardo-Acosta, S. B., Telesco, C. M., & Knacke, R. F. 1998, AJ, 115, 2101
Fajardo-Acosta, S. B., Stencel, R. E., Backman, D. E., & Thakur, N. 1999, ApJ, 520, 215
Fisher, R. S., Telesco, C. M., Piña, R. K., Knacke, R. F., & Wyatt, M. C. 2000, ApJ, 532, L141
Furlan, E., Sargent, B., Calvet, N., et al. 2007, ApJ, 664, 1176
Garcia-Lario, P., Manchado, A., Suso, S. R., Pottasch, S. R., & Olling, R. 1990, A&AS, 82, 497
Gómez de Castro, A. I. 2009, ApJ, 698, L108
Greaves, J. S., Coulson, I. M., Moriarty-Schieven, G., et al. 2000, in BAAS, 197, 826
Greaves, J. S., Holland, W. S., Wyatt, M. C., et al. 2005, ApJ, 619, L187
Greaves, J. S., Stauffer, J. R., Collier Cameron, A., Meyer, M. R., & Sheehan, C. K. W. 2009, MNRAS, 394, L36
Gregorio-Hetem, J., Lepine, J. R. D., Quast, G. R., Torres, C. A. O., & de La Reza, R. 1992, AJ, 103, 549
Güsten, R., Nyman, L. Å., Schilke, P., et al. 2006, A&A, 454, L13
Henry, T. J., Soderblom, D. R., Donahue, R. A., & Baliunas, S. L. 1996, AJ, 111, 439
Hildebrand, R. H. 1983, QJRAS, 24, 267
Hillenbrand, L. A., Carpenter, J. M., Kim, J. S., et al. 2008, ApJ, 677, 630
Holland, W. S., Greaves, J. S., Zuckerman, B., et al. 1998, Nature, 392, 788
Hollenbach, D., Gorti, U., Meyer, M., et al. 2005, ApJ, 631, 1180
Holman, M. J., & Wiegert, P. A. 1999, AJ, 117, 621
Holmes, E. K., Butner, H. M., Fajardo-Acosta, S. B., & Rebull, L. M. 2003, AJ, 125, 3334
Iorio, L. 2007, MNRAS, 375, 1311
Ivison, R. J., Greve, T. R., Dunlop, J. S., et al. 2007, MNRAS, 380, 199
Jaschek, C., Jaschek, M., Egret, D., & Andrillat, Y. 1991, A&A, 252, 229
Jayawardhana, R., Fisher, S., Hartmann, L., et al. 1998, ApJ, 503, L79
Jensen, E. L. N., Mathieu, R. D., & Fuller, G. A. 1996, ApJ, 458, 312
Jourdain de Muizon, M., Laureijs, R. J., Dominik, C., et al. 1999, A&A, 350, 875
Jura, M., Ghez, A. M., White, R. J., et al. 1995, ApJ, 445, 451
Jura, M., Zuckerman, B., Becklin, E. E., & Smith, R. C. 1993, ApJ, 418, L37
Kenyon, S. J., & Bromley, B. C. 2004, AJ, 127, 513
Kenyon, S. J., & Bromley, B. C. 2008, ApJS, 179, 451
Kessler, M. F., Steinz, J. A., Anderegg, M. E., et al. 1996, A&A, 315, L27
Koerner, D. W., Ressler, M. E., Werner, M. W., & Backman, D. E. 1998, ApJ, 503, L83
Kovács, A. 2008, in Presented at the Society of Photo-Optical Instrumentation Engineers (SPIE) Conference, Conf. Ser., 7020
Krivov, A. V., Löhne, T., & Sremčević, M. 2006, A&A, 455, 509
Laskar, T., Soderblom, D. R., Valenti, J. A., & Stauffer, J. R. 2009, ApJ, 698, 660
Lasue, J., & Levasseur-Regourd, A. C. 2006, J. Quant. Spectrosc. Radiat. Transf., 100, 220
Laureijs, R. J., Jourdain de Muizon, M., Leech, K., et al. 2002, A&A, 387, 285
Lestrade, J.-F., Wyatt, M. C., Bertoldi, F., Dent, W. R. F., & Menten, K. M. 2006, A&A, 460, 733
Li, A., & Draine, B. T. 2001, ApJ, 554, 778
Liseau, R., Brandeker, A., Fridlund, M., et al. 2003, A&A, 402, 183
Liu, M. C., Matthews, B. C., Williams, J. P., & Kalas, P. G. 2004, ApJ, 608, 526
Löhne, T., Krivov, A. V., & Rodmann, J. 2008, ApJ, 673, 1123
López-Santiago, J., Montes, D., Crespo-Chacón, I., & Fernández-Figueroa, M. J. 2006, ApJ, 643, 1160
Low, F. J., Smith, P. S., Werner, M., et al. 2005, ApJ, 631, 1170
Lowrance, P. J., Schneider, G., Kirkpatrick, J. D., et al. 2000, ApJ, 541, 390
Mamajek, E. E., & Hillenbrand, L. A. 2008, ApJ, 687, 1264
Mamajek, E. E., Meyer, M. R., & Liebert, J. 2002, AJ, 124, 1670
Mamajek, E. E., Meyer, M. R., Hinz, P. M., et al. 2004, ApJ, 612, 496
Mandell, A. M., Raymond, S. N., & Sigurdsson, S. 2007, ApJ, 660, 823
Maness, H. L., Fitzgerald, M. P., Paladini, R., et al. 2008, ApJ, 686, L25
Mannings, V., & Barlow, M. J. 1998, ApJ, 497, 330
Mannings, V., & Emerson, J. P. 1994, MNRAS, 267, 361
Manoj, P., Bhatt, H. C., Maheswar, G., & Muneer, S. 2006, ApJ, 653, 657
Matthews, B. C., Greaves, J. S., Holland, W. S., et al. 2007, PASP, 119, 842
Mentuch, E., Brandeker, A., van Kerkwijk, M. H., Jayawardhana, R., & Hauschildt, P. H. 2008, ApJ, 689, 1127
Merín, B., Montesinos, B., Eiroa, C., et al. 2004, A&A, 419, 301
Meyer, M. R., Carpenter, J. M., Mamajek, E. E., et al. 2008, ApJ, 673, L181
Miyake, K., & Nakagawa, Y. 1993, Icarus, 106, 20
Moór, A., Ábrahám, P., Derekas, A., et al. 2006, ApJ, 644, 525
Mouillet, D., Lagrange, A. M., Augereau, J. C., & Ménard, F. 2001, A&A, 372, L61
Najita, J., & Williams, J. P. 2005, ApJ, 635, 625
Neugebauer, G., Habing, H. J., van Duinen, R., et al. 1984, ApJ, 278, L1
Nilsson, R., Liseau, R., Brandeker, A., et al. 2009, A&A, 508, 1057
Peck, A. B., & Beasley, A. J. 2008, J. Phys. Conf. Ser., 131, 012049
Perryman, M. A. C., Lindegren, L., Kovalevsky, J., et al. 1997, A&A, 323, L49
Pollack, J. B., Hollenbach, D., Beckwith, S., et al. 1994, ApJ, 421, 615
Prato, L., Ghez, A. M., Piña, R. K., et al. 2001, ApJ, 549, 590
Quillen, A. C., Varnière, P., Minchev, I., & Frank, A. 2005, AJ, 129, 2481
Reach, W. T., Morris, P., Boulanger, F., & Okumura, K. 2003, Icarus, 164, 384
Rebull, L. M., Stapelfeldt, K. R., Werner, M. W., et al. 2008, ApJ, 681, 1484
Reche, R., Beust, H., & Augereau, J. 2009, A&A, 493, 661
Rhee, J. H., Song, I., Zuckerman, B., & McElwain, M. 2007, ApJ, 660, 1556
Rieke, G. H., Su, K. Y. L., Stansberry, J. A., et al. 2005, ApJ, 620, 1010
Roccatagliata, V., Henning, T., Wolf, S., et al. 2009, A&A, 497, 409
Schneider, G., Smith, B. A., Becklin, E. E., et al. 1999, ApJ, 513, L127
Schneider, G., Weinberger, A. J., Becklin, E. E., Debes, J. H., & Smith, B. A. 2009, AJ, 137, 53
Schütz, O., Meeus, G., & Sterzik, M. F. 2005, A&A, 431, 175
Shen, Y., Draine, B. T., & Johnson, E. T. 2009, ApJ, 696, 2126
Sheret, I., Dent, W. R. F., & Wyatt, M. C. 2004, MNRAS, 348, 1282
Siringo, G., Kreysa, E., Kovács, A., et al. 2009, A&A, 497, 945
Soderblom, D. R., King, J. R., Siess, L., et al. 1998, ApJ, 498, 385
Song, I., Caillault, J., Barrado y Navascués, D., & Stauffer, J. R. 2001, ApJ, 546, 352
Song, I., Zuckerman, B., & Bessell, M. S. 2003, ApJ, 599, 342
Spangler, C., Sargent, A. I., Silverstone, M. D., Becklin, E. E., & Zuckerman, B. 2001, ApJ, 555, 932
Stauffer, J. R., Hartmann, L. W., & Barrado y Navascues, D. 1995, ApJ, 454, 910
Stognienko, R., Henning, T., & Ossenkopf, V. 1995, A&A, 296, 797
Su, K. Y. L., Rieke, G. H., Stansberry, J. A., et al. 2006, ApJ, 653, 675
Su, K. Y. L., Rieke, G. H., Stapelfeldt, K. R., et al. 2008, ApJ, 679, L125
Sylvester, R. J., & Mannings, V. 2000, MNRAS, 313, 73

Sylvester, R. J., Skinner, C. J., Barlow, M. J., & Mannings, V. 1996, MNRAS, 279, 915
Sylvester, R. J., Dunkin, S. K., & Barlow, M. J. 2001, MNRAS, 327, 133
Tanner, A., Beichman, C., Bryden, G., Lisse, C., & Lawler, S. 2009, ApJ, 704, 109
Telesco, C. M., Fisher, R. S., Piña, R. K., et al. 2000, ApJ, 530, 329
Thébault, P., & Augereau, J.-C. 2007, A&A, 472, 169
Thévenin, F., & Idiart, T. P. 1999, ApJ, 521, 753
Thorén, P., & Feltzing, S. 2000, A&A, 363, 692
Torres, C. A. O., Quast, G. R., da Silva, L., et al. 2006, A&A, 460, 695
Touboul, M., Kleine, T., Bourdon, B., Palme, H., & Wieler, R. 2007, Nature, 450, 1206
Trilling, D. E., Stansberry, J. A., Stapelfeldt, K. R., et al. 2007, ApJ, 658, 1289
Trilling, D. E., Bryden, G., Beichman, C. A., et al. 2008, ApJ, 674, 1086
Uzpen, B., Kobulnicky, H. A., Monson, A. J., et al. 2007, ApJ, 658, 1264
Valenti, J. A., & Fischer, D. A. 2005, VizieR Online Data Catalog, 215, 90141
Verrier, P. E., & Evans, N. W. 2008, MNRAS, 390, 1377
Wahhaj, Z., Koerner, D. W., Backman, D. E., et al. 2005, ApJ, 618, 385
Walker, H. J., & Butner, H. M. 1995, Ap&SS, 224, 389
Walker, H. J., & Heinrichsen, I. 2000, Icarus, 143, 147
Wang, W., Cowie, L. L., & Barger, A. J. 2004, ApJ, 613, 655
Weinberger, A. J., Becklin, E. E., Schneider, G., et al. 1999, ApJ, 525, L53
Weinberger, A. J., Rich, R. M., Becklin, E. E., Zuckerman, B., & Matthews, K. 2000, ApJ, 544, 937
Weiß, A., Kovács, A., Coppin, K., et al. 2009, ApJ, 707, 1201
Werner, M. W., Roellig, T. L., Low, F. J., et al. 2004, ApJS, 154, 1
Williams, J. P., & Andrews, S. M. 2006, ApJ, 653, 1480
Williams, J. P., Najita, J., Liu, M. C., et al. 2004, ApJ, 604, 414
Wilner, D. J., Holman, M. J., Kuchner, M. J., & Ho, P. T. P. 2002, ApJ, 569, L115
Wyatt, M. C. 2005, A&A, 440, 937
Wyatt, M. C. 2008, ARA&A, 46, 339
Wyatt, M. C., Smith, R., Su, K. Y. L., et al. 2007, ApJ, 663, 365
Zuckerman, B., & Becklin, E. E. 1993, ApJ, 414, 793
Zuckerman, B., & Song, I. 2004a, ApJ, 603, 738
Zuckerman, B., & Song, I. 2004b, ARA&A, 42, 685
Zuckerman, B., & Webb, R. A. 2000, ApJ, 535, 959
Zuckerman, B., Song, I., Bessell, M. S., & Webb, R. A. 2001, ApJ, 562, L87